Supporting Information

Key Role of d^0 and d^{10} Cations for the Design of Semiconducting Colusites: Large Thermoelectric *ZT* in $Cu_{26}Ti_2Sb_6S_{32}$ compounds

Takashi Hagiwara,[a] Koichiro Suekuni,*[a,b] Pierric Lemoine,[c] Andrew R. Supka,[d] Raju Chetty,[e] Emmanuel Guilmeau,*[f] Bernard Raveau,[f] Marco Fornari,[d] Michihiro Ohta,[e] Rabih Al Rahal Al Orabi,[d] Hikaru Saito,[g] Katsuaki Hashikuni,[a] and Michitaka Ohtaki[a,b]

[a] Department of Applied Science for Electronics and Materials, Interdisciplinary Graduate School of Engineering Sciences, Kyushu University, Kasuga, Fukuoka 816–8580, Japan
*suekuni.koichiro.063@m.kyushu-u.ac.jp
[b] Transdisciplinary Research and Education Center for Green Technologies, Kyushu University, Kasuga, Fukuoka 816-8580, Japan
[c] Université de Rennes 1, CNRS, ISCR-UMR 6226, F-35000 Rennes, France
[d] Department of Physics and Science of Advanced Materials Program, Central Michigan University, Mt. Pleasant, Michigan 48859, USA
[e] Global Zero Emission Research Center, National Institute of Advanced Industrial Science and Technology (AIST), Tsukuba, Ibaraki 305-8569, Japan
[f] CRISMAT, CNRS, Normandie Université, ENSICAEN, UNICAEN, 14000 Caen, France
*emmanuel.guilmeau@ensicaen.fr
[g] Institute for Materials Chemistry and Engineering, Kyushu University, Kasuga, Fukuoka 816-8580, Japan

Table S1. Hubbard *U* (eV) correction computed with the ACBN0 approach.

Ti	Cu (12f)	Cu (6d)	Cu (8e)	Sb	S (24i)	S (8e)	Ge
0.009	7.995	7.565	7.780	0.005	1.483	1.643	0.003

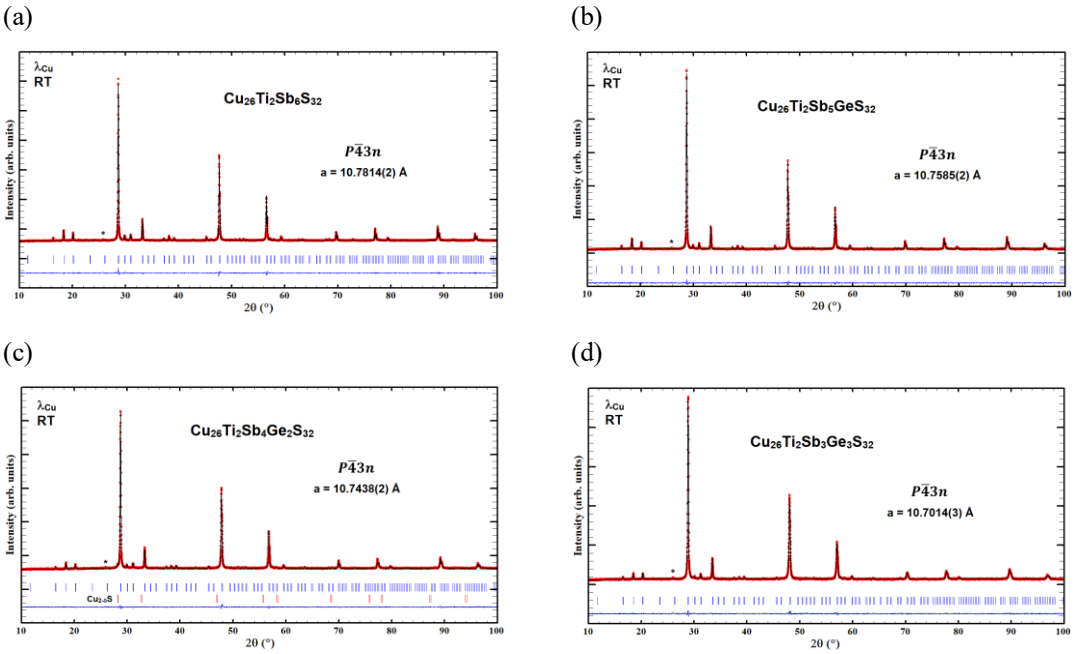

Figure S1. Rietveld refinements of powder X-ray diffraction patterns recorded at room temperature of: a) $Cu_{26}Ti_2Sb_6S_{32}$ (R_{Bragg} = 4.27, R_F = 9.29, R_{wp} = 4.67, R_{exp} = 5.97, χ^2 = 0.612), b) $Cu_{26}Ti_2Sb_5GeS_{32}$ (R_{Bragg} = 1.71, R_F = 3.54, R_{wp} = 4.10, R_{exp} = 5.78, χ^2 = 0.503), c) $Cu_{26}Ti_2Sb_4Ge_2S_{32}$ (R_{Bragg} = 2.51, R_F = 4.23, R_{wp} = 4.11, R_{exp} = 5.75, χ^2 = 0.510), and d) $Cu_{26}Ti_2Sb_3Ge_3S_{32}$ (R_{Bragg} = 1.80, R_F = 3.60, R_{wp} = 3.93, R_{exp} = 5.47, χ^2 = 0.517).

Table S2. Rietveld refinement result for powder X-ray diffraction pattern of $Cu_{26}Ti_2Sb_6S_{32}$. The interatomic distances of $Cu_{26}Ti_2Sb_6S_{32}$ are compared with those of $Cu_{26}V_2Sn_6S_{32}$[S1] and $Cu_{26}T_2Ge_6S_{32}$ (T = Cr, Mo, W)[S2] colusites.

Atom	site	x	y	z	B_{iso}
Ti	2a	0	0	0	1.03(29)
Sb	6c	1/4	1/2	0	0.80(6)
Cu	6d	1/4	0	1/2	1.80(14)
Cu	8e	0.246(1)	x	x	1.16(14)
Cu	12f	0.256(1)	0	0	0.93(10)
S	8e	0.122(1)	x	x	-0.28(46)
S	24i	0.377(1)	0.366(1)	0.132(1)	0.59(20)

$Cu_{26}T_2M_6S_{32}$ Distances	T = Ti, M = Sb	T = V, M = Sn	T = V, M = Ge	T = W, M = Ge	T = Mo, M = Ge	T = Cr, M = Ge
T(2a)-S(8e) ×4	2.271 Å	2.390 Å	2.247 Å	2.343 Å	2.351 Å	2.218 Å
T(2a)-Cu(12f) ×6	2.763 Å	2.736 Å	2.739 Å	2.763 Å	2.752 Å	2.709 Å
M(6c)-S(24i) ×4	2.451 Å	2.422 Å	2.248 Å	2.213 Å	2.229 Å	2.230 Å
Cu(6d)-S(24i) ×4	2.313 Å	2.254 Å	2.287 Å	2.313 Å	2.291 Å	2.291Å
Cu(8e)-S(8e) ×1	2.327 Å	2.357 Å	2.376 Å	2.407 Å	2.332 Å	2.365 Å
Cu(8e)-S(24i) ×3	2.276 Å	2.277 Å	2.272 Å	2.273 Å	2.280 Å	2.271 Å
Cu(12f)-S(8e) ×2	2.355 Å	2.377 Å	2.333 Å	2.377 Å	2.373 Å	2.307 Å
Cu(12f)-S(24i) ×2	2.297 Å	2.330 Å	2.298 Å	2.288 Å	2.295 Å	2.306 Å
Average Cu-S	2.309 Å	2.302 Å	2.300 Å	2.317 Å	2.306 Å	2.297 Å

(S1) Bourgès, C.; Bouyrie, Y.; Supka, A. R.; Al Rahal Al Orabi, R.; Lemoine, P.; Lebedev, O. I.; Ohta, M.; Suekuni, K.; Nassif, V.; Hardy, V.; Daou, R.; Miyazaki, Y.; Fornari, M.; Guilmeau, E. High-Performance Thermoelectric Bulk Colusite by Process Controlled Structural Disordering. *J. Am. Chem. Soc.* **2018**, 140, 2186– 2195.

(S2) Pavan Kumar, V.; Supka, A. R.; Lemoine, P.; Lebedev, O. I.; Raveau, B.; Suekuni, K.; Nassif, V.; Al Rahal Al Orabi, R.; Fornari, M.; Guilmeau, E. High Power Factors of Thermoelectric Colusites $Cu_{26}T_2Ge_6S_{32}$ (T = V, Cr, Mo, W): Toward Functionalization of the Conductive "Cu–S" Network. *Adv. Energy Mater.* **2019**, 9, 1803249.

Table S3. Chemical compositions for the sintered samples of $Cu_{26}Ti_2Sb_{6-x}Ge_xS_{32}$. The standard deviation of the composition is given in the parentheses. As known for all sulfides, the determination of the sulfur content by EDS is not accurate. Thus, the value of about 29 S is in the limit of the experimental errors that can be estimated to ~10% with respect to 32 S determined from the structural analysis. Consequently, the "observed" S deficiency cannot be considered as significant and moreover is inconsistent with the p-type semiconducting behavior of $Cu_{26}Ti_2Sb_6S_{32}$.

	Cu	Ti	Sb	Ge	S
$x = 0$	25.9(2)	1.9(1)	6.2(2)	—	29.5(5)
$x = 1$	26.0(3)	1.9(1)	5.2(2)	0.9(3)	29.4(5)
$x = 2$	26.1(4)	1.9(2)	4.2(3)	1.8(4)	29.4(6)
$x = 3$	26.3(3)	1.9(1)	3.1(1)	2.7(3)	29.5(4)

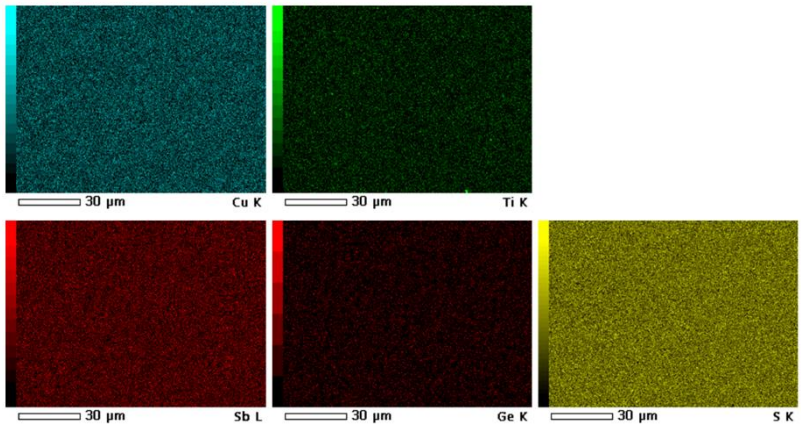

Figure S2. Elemental mapping of energy dispersive spectroscopy for $Cu_{26}Ti_2Sb_{6-x}Ge_xS_{32}$ ($x = 2$).

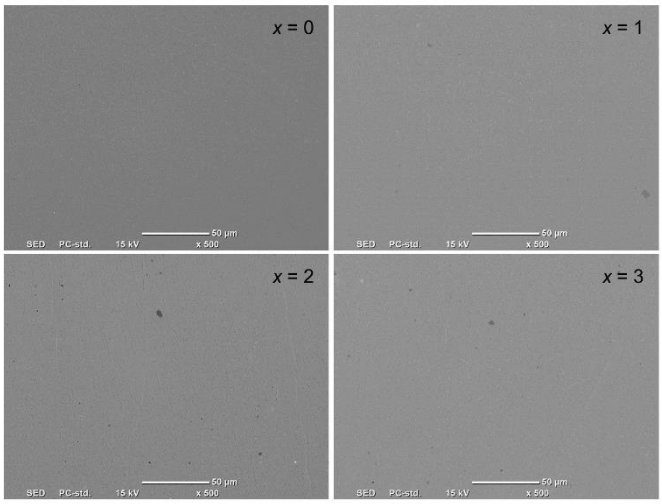

Figure S3. Scanning electron microscope images for $Cu_{26}Ti_2Sb_{6-x}Ge_xS_{32}$ ($x = 0$–3).

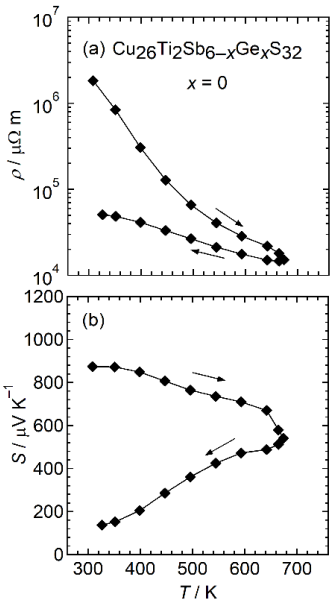

Figure S4. (a) Electrical resistivity ρ and (b) Seebeck coefficient S for $Cu_{26}Ti_2Sb_{6-x}Ge_xS_{32}$ (x = 0).

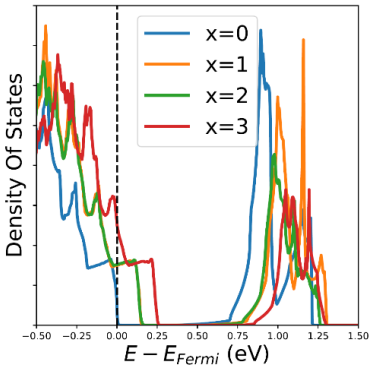

Figure S5. Electronic density of states of $Cu_{26}Ti_2Sb_{6-x}Ge_xS_{32}$ (x = 0–3).

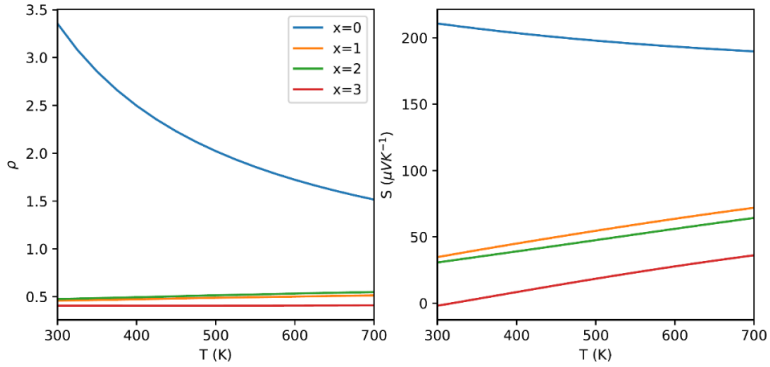

Figure S6. Electrical resistivity ρ and Seebeck coefficient S of $Cu_{26}Ti_2Sb_{6-x}Ge_xS_{32}$ (x = 0–3) calculated based on the electronic structure (Figure 3 in the main text and Figure S5).

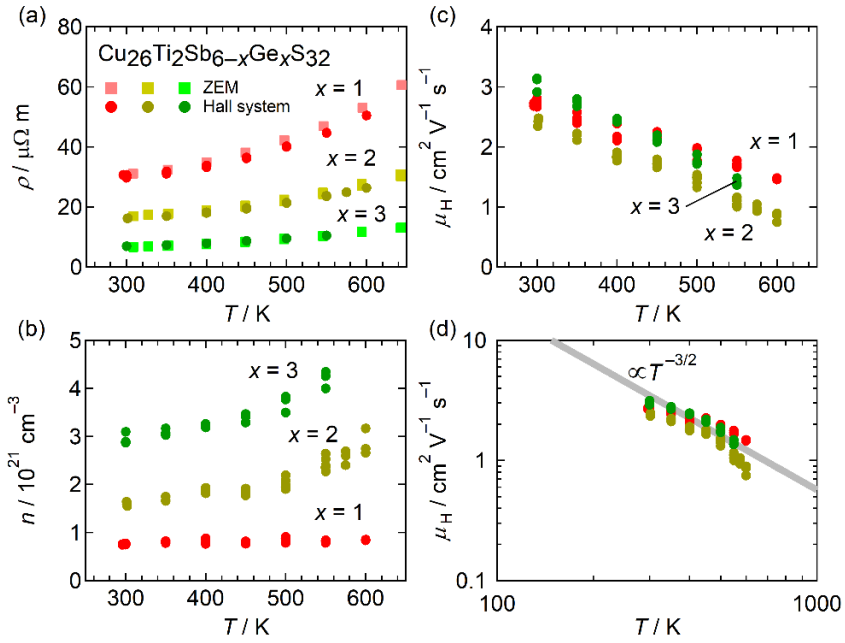

Figure S7. (a) Electrical resistivity ρ, (b) hole carrier concentration n, and (c, d) Hall mobility μ_H for $Cu_{26}Ti_2Sb_{6-x}Ge_xS_{32}$ (x = 1–3). The data μ_H fall on a $\propto T^{-3/2}$ line.

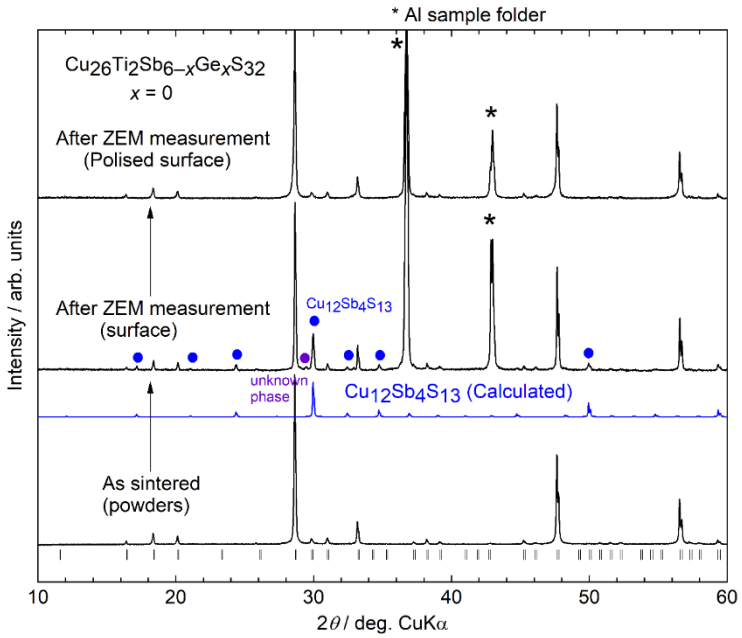

Figure S8. Powder X-ray diffraction patterns for $Cu_{26}Ti_2Sb_{6-x}Ge_xS_{32}$ (x = 0). After the measurement of the electrical resistivity ρ and Seebeck coefficient S (Figure S4), $Cu_{12}Sb_4S_{13}$ and an unknown phase appeared at a surface of the sample. The secondary phases can be removed by polishing. A calculated pattern for $Cu_{12}Sb_4S_{13}$ is also shown.

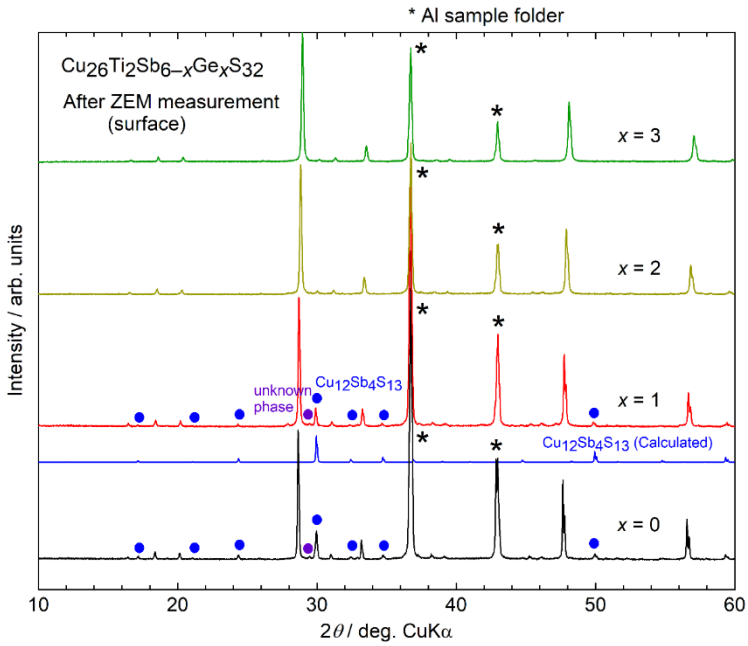

Figure S9. Powder X-ray diffraction patterns measured on the surface of $Cu_{26}Ti_2Sb_{6-x}Ge_xS_{32}$ (x = 0–3) samples after the measurement of the electrical resistivity ρ and Seebeck coefficient S (Figure 4).

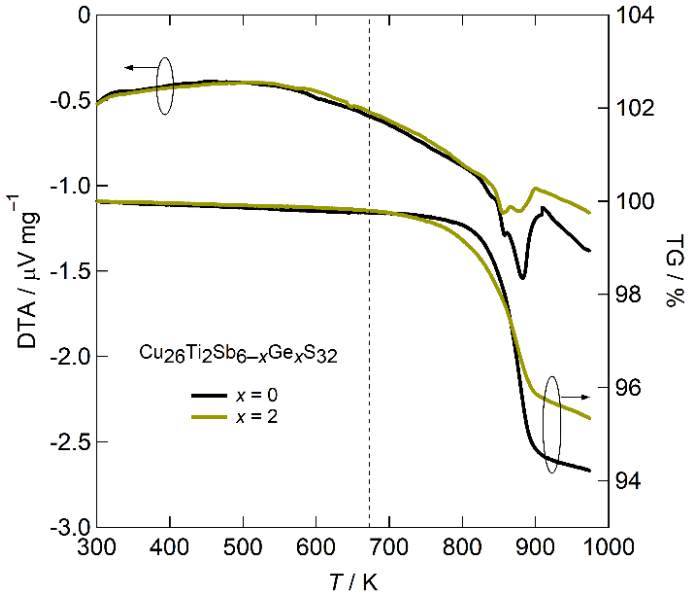

Figure S10. Thermogravimetry/differential thermal analysis data for $Cu_{26}Ti_2Sb_{6-x}Ge_xS_{32}$ (x = 0, 2). Endothermic peaks accompanied by mass reduction were observed at around 850 K.

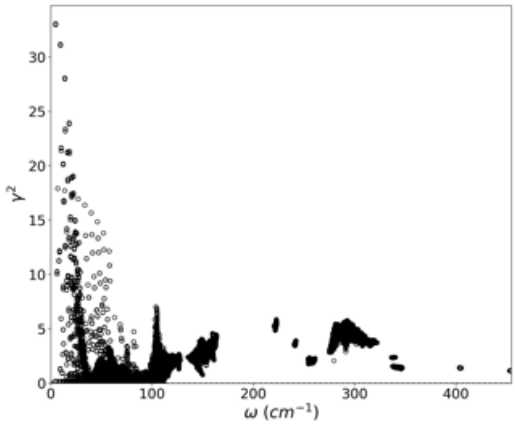

Figure S11. Mode-resolved Grüneisen parameters of $Cu_{26}Ti_2Sb_6S_{32}$ calculated based on the phonon structure (Figure 5 in the main text).